Sustainable Energy & Fuels

Accepted Manuscript

This article can be cited before page numbers have been issued, to do this please use: A. Sartorel, G. A. Volpato, A. Bonetto, A. Marcomini, P. Mialane, M. Bonchio and M. Natali, *Sustainable Energy Fuels*, 2018, DOI: 10.1039/C8SE00275D.

ROYAL SOCIETY OF CHEMISTRY

rsc.li/sustainable-energy

View Article Online
DOI: 10.1039/C8SE00275D

Journal Name

ARTICLE

Proton coupled electron transfer from Co_3O_4 nanoparticles to photogenerated $Ru(bpy)_3^{3+}$: base catalysis and buffer effect

Received 00th January 20xx,
Accepted 00th January 20xx

DOI: 10.1039/x0xx00000x

www.rsc.org/

Giulia Alice Volpato,[a] Alessandro Bonetto,[b] Antonio Marcomini,[b] Pierre Mialane,[c] Marcella Bonchio,[a] Mirco Natali*[d] and Andrea Sartorel*[a]

Co_3O_4 nanoparticles in the spinel crystalline structure are among the most promising catalysts for the water oxidation reaction, displaying remarkable activity under electrochemical and light-assisted conditions. In the presence of $Ru(bpy)_3^{2+}$ as photosensitizer (bpy = 2,2'-bipyridine) and $Na_2S_2O_8$ as electron acceptor, 5±1 nm size Co_3O_4 nanoparticles show a slow primary electron transfer (ET) to photogenerated Ru(III), occurring in a timescale of tens of milliseconds. We demonstrate herein that: (i) photo-oxidation of Co_3O_4 NPs by Ru(III) involves transformation of surface Co(III)-OH sites to formal Co(IV)=O, along a proton-coupled electron-transfer (PCET) pathway; (ii) the rate of the process depends on pH, on the nature and concentration of the buffer; (iii) borate promotes general base catalysis of the PCET; (iv) inhibition of the PCET is observed at high buffer concentration, due to H_3BO_3 poisoning of the surface Co sites, resulting in depletion of the O_2 evolution activity.

Introduction

The development of efficient water oxidation catalysts (WOCs) has been the subject of intensive research in the last decade. Since the pioneering studies by Harriman,[1] cobalt oxide nanoparticles (NPs) have been recognized as very active WOCs, displaying low operating overpotentials (η = 0.30 - 0.40 V)[2,3,4,5] and residing close to the top of the Volcano plot for metal oxides,[6] while promoting fast catalysis (turnover frequency (TOF) up to 3 s^{-1} per surface catalytic site).[3,7]

In addition, cobalt oxide NPs, in the Co_3O_4 cubic spinel crystalline structure, have been employed as WOCs in light activated sacrificial systems employing photogenerated $Ru(bpy)_3^{3+}$ oxidant,[8,9,10,11,12] with quantum yield up to 0.07,[13] and spectroscopic evidence of Co(III)-OH moieties as the active surface sites.[7] Investigation of such light-activated systems may lead to important mechanistic information on the catalyst evolution along the oxygenic cycle.[14–16] In particular, we have recently reported that Co_3O_4 NPs, either without stabilizing ligands or capped with bisphosphonate alendronate pendants, suffer from a slow electron transfer (ET) to photogenerated $Ru(bpy)_3^{3+}$, occurring in a timescale of tens of milliseconds,[13] resulting several orders of magnitude slower than ET observed with molecular Co complexes.[17–20,21] Slow ET rates may impact on the performance of light-activated systems, in particular when the catalyst is embedded in dye-sensitized photoelectrodes.[22,23] In this work, we take advantage of laser flash photolysis studies to investigate the mechanistic origin of such photoinduced ET process involving surface sites of Co_3O_4 NPs. Relevant observations are: i) the attribution of this process to a proton-coupled electron-transfer (PCET) involving oxidation of Co(III)-OH sites to Co(IV)=O, by comparison with $CoFe_2O_4$ spinel nanoparticles (30 nm size); ii) the impact of the solution buffer on the primary PCET event; iii) a general base catalysis effect of borate buffer along the PCET; iv) the inhibition of the PCET process and abatement of O_2 evolution activity at high buffer concentration, likely ascribable to H_3BO_3 coordination to surface sites.

Results and discussion

Co_3O_4 NPs with 5±1 nm size were synthesized as previously described,[13] using the procedure by Niederberger et al;[12] see characterization in the ESI (Fig. S1-S4†) and in reference 13.

We examined by laser flash photolysis the ability of Co_3O_4 NPs (100 μM formal concentration)[13] in giving ET to $Ru(bpy)_3^{3+}$, photogenerated in few ns upon laser excitation of 50 μM $Ru(bpy)_3^{2+}$ in the presence of 5 mM $Na_2S_2O_8$, in 0.004-0.4 M borate buffer at pH 8.0-9.5 (the concentration refers to the $H_3BO_3/B(OH)_4^-$ acid/base couple, pK_a = 8.6[24]), see eqs 1-4.[13]

$$\mathbf{Ru(II)(bpy)_3^{2+}} + h\nu \rightarrow \mathbf{{}^*Ru(II)(bpy)_3^{2+}} \quad (1)$$

[a] Department of Chemical Sciences University of Padova and Institute on Membrane Technology, Unit of Padova, via F. Marzolo 1, Padova, 35131, Italy.
[b] Dept. Environmental Sciences, Informatics and Statistics, University Ca' Foscari Venice, Vegapark, Via delle Industrie 21/8, 30175 Marghera, Venice, Italy.
[c] Institut Lavoisier de Versailles, UMR 8180, Université Paris-Saclay, Université de Versailles Saint-Quentin en Yvelines, 45 Avenue des Etats-Unis Versailles cedex, 78035, France.
[d] Department of Chemical and Pharmaceutical Sciences, University of Ferrara, Via L. Borsari 46, Ferrara, 44121, Italy.

† Footnotes relating to the title and/or authors should appear here.
Electronic Supplementary Information (ESI) available: [characterization of Co_3O_4 NPs, additional electrochemical and photophysical experiments]. See DOI: 10.1039/x0xx00000x

View Article Online
DOI: 10.1039/C8SE00275D

$$*Ru(II)(bpy)_3^{2+} + S_2O_8^{2-} \rightarrow Ru(III)(bpy)_3^{3+} + SO_4^{\cdot-} + SO_4^{2-} \quad (2)$$
$$Ru(II)(bpy)_3^{2+} + SO_4^{\cdot-} \rightarrow Ru(III)(bpy)_3^{3+} + SO_4^{2-} \quad (3)$$
$$Ru(III)(bpy)_3^{3+} + Co_3O_4 \rightarrow Ru(II)(bpy)_3^{2+} + Co_3O_4(h^+) \quad (4)$$

The laser-induced generation of Ru(III) (eqs 1-3) is associated to the prompt formation of a negative ΔOD at 450 nm (bleaching of the MLCT ground-state absorption, indicative of Ru(II)→Ru(III) transformation by photoinduced oxidative quenching with persulfate) and occurs within ca 10 μs.[16,21] The progressive increase of the ΔOD^{450} (bleach recovery, see traces in Fig. 1) is then representative of the occurrence of the reduction of Ru(III) to Ru(II) by Co_3O_4 NPs (eq 4).[16,21]

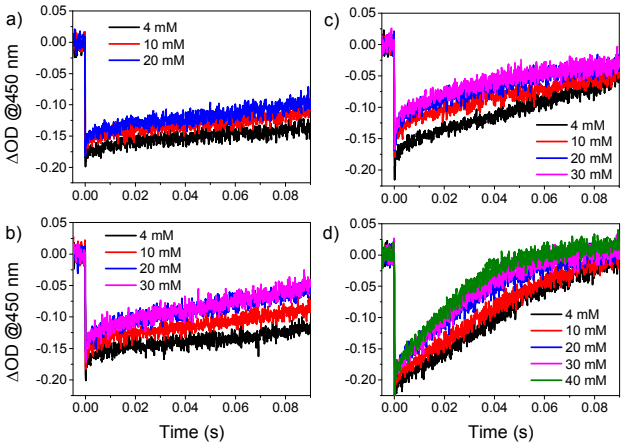

Figure 1. Laser flash photolysis (λ_{exc} = 355 nm) of 50 μM $Ru(bpy)_3^{2+}$ in the presence of 5 mM $Na_2S_2O_8$ and 100 μM Co_3O_4 NPs in: (a) 4-20 mM borate buffer, pH 8.0; (b) 4-30 mM borate buffer, pH 8.5; (c) 4-30 mM borate buffer, pH 8.9; and (d) 4-40 mM borate buffer, pH 9.5.

Concerning the nature of the sites involved in such ET to $Ru(bpy)_3^{3+}$, both tetrahedral Co(II) and octahedral Co(III) sites of the Co_3O_4 spinel structure could be considered.[4,25,26] Different Co(III)-OH surface sites were envisaged based on time resolved rapid-scan infrared spectroscopy,[7] with fast catalytic sites being characterized by the presence of a second, neighbouring, dioxo bridged Co(III)-OH moiety (Fig. 2).[7] Moreover, Co_3O_4 NPs are also known to form amorphous cobaltate clusters at the surface, featuring dicobalt edge active sites (Fig. 2).[24] §

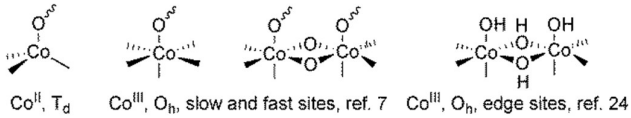

Figure 2. Possible surface sites of Co_3O_4 NPs involved in ET to $Ru(bpy)_3^{3+}$.

We thus performed a control flash photolysis experiment with commercially available 30 nm size $Co^{II}Fe^{III}{}_2O_4$ NPs, having still spinel crystalline structure with tetrahedral Co(II) and octahedral Fe(III) sites. The silent trace observed (figure S5†) clearly suggests that Co(II) are not reactive towards Ru(III) in this timescale,§§ and thus indicates that the Co(III) surface sites are those involved in the reduction of $Ru(bpy)_3^{3+}$.

Looking into more details at the kinetic traces in Fig. 1, the rate and the amount of the ΔOD^{450} recovery in a timescale of ca 90 ms were found to be dependent on the pH and on the concentration of the buffer. Typically, the rate of the ΔOD^{450} recovery is first order in Ru(III) concentration and is thus expressed by eq. 5.

$$Rate = -d[Ru(III)]/dt = k_{obs} \times [Ru(III)] \quad (5)$$

In the present case, however, the traces were not accurately fitted with single-exponential decays associated to eq. 5. Non-exponential kinetics were observed for photoinduced proton-coupled electron-transfer (PCET) involving ZnO nanocrystals, and were attributed to the presence of different type of subsurface and surface sites.[27] Moreover, in the present case, difficulties in fitting the traces are also due to a low recovery of the ΔOD^{450} bleach in the instrumental timescale limit of ca 90 ms (see Fig. 1a), and to the impossibility of investigating the system under pure pseudo-first order conditions with respect to photogenerated Ru(III).‡ Indeed, under optimized conditions, photogenerated Ru(III) concentration is ~2×10^{-5} M, while surface sites potentially involved in the PCET process are ~2.5×10^{-5} M, being estimated as ¼ of the total formal concentration of Co_3O_4 NPs = 10^{-4} M.[13] We thus estimated the kinetic constant k_{obs} of the process from the reciprocal of the Ru(III) lifetime according to eq. 6, where τ is experimentally determined at half recovery of the ΔOD^{450} in the experimental traces.♦ The determined values of τ and of k_{obs} in the different conditions are reported in table S1†. For the sake of comparison, we have also included the τ and k_{obs} values derived from single or multi-exponential fitting of the traces, that lead to a good match with the values determined as described above (see Table S1† and S2†).

$$k_{obs} = \ln(2)/\tau \quad (6)$$

k_{obs} was observed to increase upon increasing both the pH and the total buffer concentration (Fig. 3). At each pH investigated, linear correlations were observed by plotting k_{obs} vs. the concentration of the $B(OH)_4^-$ base in solution, with the latter given by [Base] = $f_B \times$[buffer], where f_B is the fraction of the $B(OH)_4^-$ basic form of the buffer, and [buffer] is the total buffer concentration (Fig. 3).[28,29,30] These results suggest a general base catalysis by $B(OH)_4^-$, assisting deprotonation of surface oxygen sites along a PCET process.[31,32] A similar observation was previously documented for the amorphous cobalt oxide (CoPi) under electrocatalytic conditions, where Co(III)-OH surface sites convert into Co(IV)=O.[33]♣ Importantly, this PCET transformation is also postulated as the primary event in the water oxidation cycle by Co_3O_4 NPs.[7] The general base catalysis associated to the Co(III)-OH → Co(IV)=O PCET is expected on the basis of the predicted change in pK_a of the surface OH group upon oxidation of the cobalt centre. According to the libido rule,[34] the pK_a of the acid/base couple (pK_a=8.6 for $H_3BO_3/B(OH)_4^-$) has to be intermediate between the pK_a of Co(III)-OH and Co(IV)-OH groups. The general kinetic law for the PCET can thus be expressed according to eq. 7, where k_B is

View Article Online
DOI: 10.1039/C8SE00275D

the rate-constant for the base assisted process and k_0 (eq 8) represents the rate constant for the PCET under unbuffered conditions (i.e., with both water and OH^- acting as base).

$$k_{obs} = k_0 + k_B \times [B] \quad (7)$$
$$k_0 = k_{H_2O} + k_{OH} \times [OH^-] \quad (8)$$

According to eq 7, the rate constants k_0 and k_B can be determined from the fitting of the data in Fig. 3 (see table 1). As expected, k_B values obtained under different pH conditions fall in an appreciably narrow range of 6.3-8.5×10^2 $M^{-1}s^{-1}$ (table 1). Importantly, experiments conducted in deuterated medium (figure S6†) show a lower k_B value of 4.9±1.0 ×10^2 $M^{-1}s^{-1}$, corresponding to a kinetic isotope effect, KIE = $k_B(H)/k_B(D)$ = 1.4±0.3. The small isotope effect is indicative of a low modification of the overlap integrals of the donor-acceptor states along the proton transfer coordinate by replacing H with D.[35] Interestingly, values comprised between 1.6 and 2.7 were observed for PCET involving Mn-oxides assisted by substituted pyridines.[36]

Concerning k_0, its value is pH dependent, as expected due to separate contributions of H_2O and OH^- acting as base (eq. 8). From a linear fitting of k_0 vs [OH^-], values of k_{H_2O} = 1.7 s^{-1} and k_{OH} = 5.5 ×10^5 $M^{-1}s^{-1}$ can be estimated (Fig. S7†).

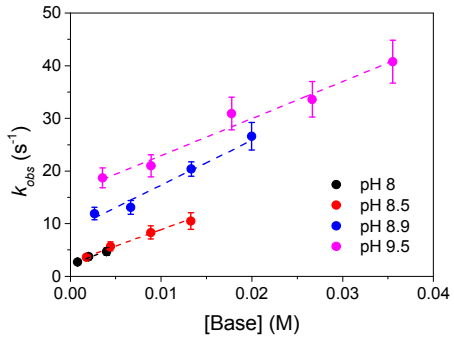

Figure 3. Plot of k_{obs} vs. [Base], where Base is $B(OH)_4^-$, and the concentrations are given by [Base]=f_B×[buffer], where f_B is the fraction of the basic form of the buffer in solution, and [buffer] is the total buffer concentration;[29] pK_a for the $H_3BO_3/B(OH)_4^-$ couple = 8.6. For k_{obs} values at pH 8 the error bars are smaller than the circles and are thus not visible in the graph (see Table S1 in the ESI).

Table 1. Kinetic rate constants for PCET from Co_3O_4 NPs to $Ru(III)(bpy)_3^{3+}$ determined by flash photolysis experiments. Errors are given from the associated linear fittings (see fig. 3).

pH	k_0, s^{-1}	$k_B/10^2$, $M^{-1}s^{-1}$
8.0	2.3±0.2	6.3±0.9
8.5	2.6±0.2	6.3±0.5
8.9	8.8±0.5	8.5±1.2
9.5	15.9±1.1	7.0±0.7
8.6[(a)]	3.4±1.0	4.9±1.0

[a]In deuterated solvent; pD was calculated according to the equation pD = 0.929×pH_{meas}+0.42, where pH_{meas} is the measured pH of the deuterated solution, with a pH-meter calibrated with non deuterated standard buffers.[24,37]

The general base catalysis in photoinduced PCET from Co_3O_4 NPs to Ru(III) is observed also employing phosphate buffer (pK_a = 7.2 for $H_2PO_4^-/HPO_4^{2-}$ couple), where k_B = 1.7±0.2 ×10^3 $M^{-1}s^{-1}$ and 2.2±0.6 ×10^3 $M^{-1}s^{-1}$ with k_0 = 1.9±0.5 s^{-1} and 5.8±1.8 s^{-1} were determined at pH = 8.0 and 8.9, respectively (see ESI, Fig. S8†). As a third probe, flash photolysis experiments in bicarbonate buffer, pH 8, show almost silent traces at 5-100 mM buffer concentrations (Fig. S9†). This evidence can be attributed to the lower basicity of HCO_3^- (pK_a = 6.3) and therefore to the reduced ability of bicarbonate to assist the PCET on Co_3O_4 (a k_B ~90 $M^{-1}s^{-1}$ can be roughly determined from the kinetic treatment of the associated flash photolysis traces, Fig. S9†). However, it is worth noting that the k_B values attained employing different bases do not follow a clear trend as a function of the pK_a.[29] This can be possibly explained by a specific, coordinating effect of the solution buffering species on the cobalt oxide surface.

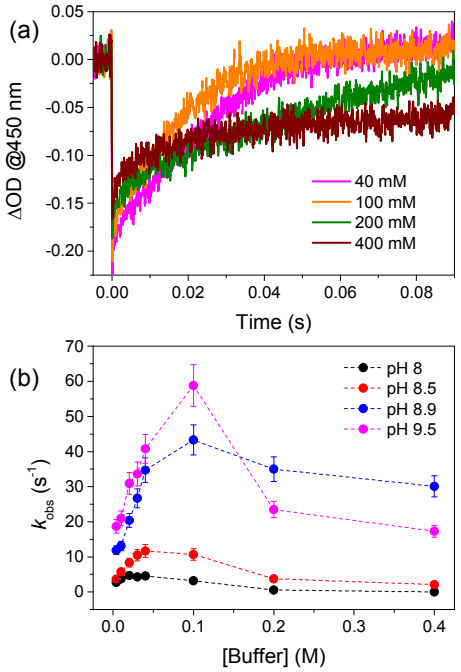

Figure 4. Top: laser flash photolysis (λ_{exc} = 355 nm) of 50 μM $Ru(bpy)_3^{2+}$ in the presence of 5 mM $Na_2S_2O_8$ and 100 μM Co_3O_4 NPs in 0.04 - 0.4 M borate buffer at pH 9.5; Bottom: plot of k_{obs} vs borate buffer concentration, under the different pH conditions investigated. For k_{obs} values at pH 8 the error bars are smaller than the circles and are not visible (see Table S1 in the ESI).

Importantly, a secondary effect on the PCET kinetics is observed at higher borate buffer concentration, see as a representative case the range 0.04-0.4 M at pH 9.5 in Figure 4a (see Fig. S10† in ESI for traces at pH values between 8.0-8.9). The most evident feature associated to these traces is that both the rate and amount of bleach recovery progressively decrease upon increasing buffer concentration (Fig. 4). The detrimental effect of highly concentrated buffer on the PCET process may be ascribed to coordination of borate species to surface Co(III) sites by replacing OH ligands,[38] thus hampering the possibility to access the PCET event. The plot of the derived k_{obs} values vs. total buffer concentration (Fig. 4b) shows indeed a clear inhibition effect by borate. This

View Article Online
DOI: 10.1039/C8SE00275D

phenomenon is more evident at lower pH, where the abatement of the k_{obs} values occurs at lower buffer concentration (Fig. 4b). This indicates that coordinatively unsaturated H_3BO_3, rather than saturated $B(OH)_4^-$, is most likely responsible for the poisoning of the Co_3O_4 surface sites. This is in in agreement with previous observations by Ullman et al. dealing with water oxidation electrocatalysis by amorphous cobalt oxide films,[24] where H_3BO_3 coordination led to inhibition of the water oxidation electrocatalysis. Consistently, an abatement of the oxygen evolution performance by Co_3O_4 NPs within the photoactivated $Ru(bpy)_3^{2+}/S_2O_8^{2-}$ catalytic cycle was observed by increasing the concentration of borate buffer from 0.08 to 0.4 M, at pH 8 (Fig. 5). This is associated to a drop of both the initial rate R_0 (7.6±0.2, 5.5±0.2, and 3.0±0.7 $\times 10^{-3}$ $\mu mol(O_2)s^{-1}$ at 0.08, 0.2, and 0.4 M borate, respectively) and the total amount of evolved O_2 (26.0±0.4 μmol, 17.0±1.0 μmol, and 7.8±0.6 μmol at 0.08, 0.2, and 0.4 M borate, respectively. These values correspond to 70±1, 46±2, and 20±2 chemical yield (CY) based on the amount of $Na_2S_2O_8$.

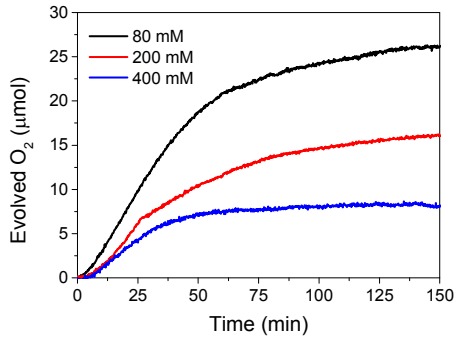

Figure 5. Oxygen evolution kinetics with 1 mM $Ru(bpy)_3^{2+}$ in the presence of 5 mM $Na_2S_2O_8$ and 165 μM formal concentration of Co_3O_4 NPs at pH 8 in 80-400 mM borate buffer. Experiments were conducted in triplicates in 15 mL total volume, irradiation was performed using a white LED light (power density 3.8 $mWcm^{-2}$).

Conclusions

The primary electron transfer from Co_3O_4 NPs (5±1 nm diameter) to photogenerated $Ru(bpy)_3^{3+}$, namely the first event in photo-assisted water oxidation by Co_3O_4, has been investigated in borate buffer solutions by laser flash photolysis technique. Such a process involves a proton coupled oxidation of the surface Co(III)-OH sites to Co(IV)=O and is assisted by general base catalysis by the $B(OH)_4^-$ base (k_B = 6.3-8.5$\times 10^2$ $M^{-1}s^{-1}$; KIE = 1.4±0.3). Higher borate buffer concentrations inhibit the PCET process, likely due to coordination of H_3BO_3 to surface sites. Consistently, an abatement of the oxygen evolving activity within the photoactivated $Ru(bpy)_3^{2+}/S_2O_8^{2-}$ cycle was observed upon increasing buffer concentration. Overall, the results presented herein further confirm the importance of specific buffer/solvent conditions on the surface reactivity of metal-oxide NPs. Therefore, benchmarking of water oxidation catalysis should take into consideration that favourable mechanistic pathways can also originate from a tailored choice of the reaction environment.

Experimental

Instrumentation and procedures.

Nanosecond transient measurements were performed with a custom laser spectrometer comprised of a Continuum Surelite II Nd:YAG laser (FWHM 6–8 ns) with frequency doubled (532 nm, 330 mJ), or tripled (355 nm, 160 mJ), option, an Applied Photophysics xenon light source including a mod. 720 150 W lamp housing, a mod. 620 power controlled lamp supply and a mod. 03-102 arc lamp pulser. Laser excitation was provided at 90° with respect to the white light probe beam. Light transmitted by the sample was focused onto the entrance slit of a 300 mm focal length Acton SpectraPro 2300i triple grating, flat field, double exit monochromator equipped with a photomultiplier detector (Hamamatsu R3896) and a Princeton Instruments PIMAX II gated intensified CCD camera, using a RB Gen II intensifier, a ST133 controller and a PTG pulser. Signals from the photomultiplier (kinetic traces) were processed by means of a TeledyneLeCroy 604Zi (400 MHz, 20 GS/s) digital oscilloscope.

Light driven catalytic tests for water oxidation were conducted in a home-made glass reactor, equipped with a FOXY oxygen selective probe from Ocean Optics inserted in the headspace, for real time monitoring of evolved O_2. 15 mL of aqueous buffer were inserted in the reactor, which was then closed and purged under dark atmosphere with nitrogen for 30 minutes: after purging, the solution was allowed to equilibrate in the dark for 10 minutes and then illuminated with a white LED spotlight (power density 3.8 $mWcm^{-2}$).

Inductively coupled plasma mass spectrometry (ICP-MS) analysis was performed by double channel Universal Cell (sp-ICP-MS NexION 350X, Perkin Elmer). In order to remove the polyatomic interference in the mass ^{59}Co (CaO), the analysis was performed in KED mode as He as carrier gas. Samples were quantified by external calibration method using a multi-point curve (6 points over the concentration range 0.1 μg L^{-1} to 50 μg L^{-1} for Ruthenium and 5 points over the concentration range 50 μg L^{-1} to 5000 μg L^{-1} for Cobalt. Yttrium at 5 $\mu g \cdot L^{-1}$ was used as internal standard. Potential contamination from the laboratory was controlled by adding at least one reagent blank during the digestion session. The limit of detection (LOD) were calculated for each sample set as the average of blanks + 3 standard deviation (SD) and is 0.66 $ng \cdot L^{-1}$ for Cobalt. The background concentration signal BEC (providing the actual magnitude of noise) detected for Cobalt was 0.001 $ng \cdot L^{-1}$. Microwave digestion of the samples were performed by using a Discover SP-D oven (CEM Corporation); each sample was added to Discover SP-D 35 mL vessel and a total of 4 mL of ultra-pure aqua regia was added. The digestion parameters are ramp time: 5 minutes, hold time: 2 minutes, digestion time: 170°C. Afterwards, the samples were allowed to cool down for 30 minutes at room temperature and properly diluted with MilliQ water.

View Article Online
DOI: 10.1039/C8SE00275D
Journal Name ARTICLE

Synthesis of Co_3O_4.[12,13] Co_3O_4 nanoparticles were prepared by dissolving cobalt(II) acetate in benzyl alcohol and heating the solution at reflux (T = 165 °C) after adding NH_3 25%. After cooling to room temperature, the Co_3O_4 NPs were washed via centrifugation–redispersion cycles with ethanol. ICP-MS: Co 75.1% (calc. for Co_3O_4 73.4%). Zeta potential analysis (1 mg/mL suspended in water) indicates a positive value of 16 mV of the apparent potential. ATR-IR: ν (cm^{-1}): 658, 555 (Co-O).

Conflicts of interest

There are no conflicts to declare.

Acknowledgements

CaRiPaRo Foundation is gratefully acknowledged for Starting Grants 2015 (AMYCORES) and for the PhD grant of GAV at the Doctoral Course in Science and Engineering of Materials and Nanostructures, University of Padova, Italy.

Notes and references

§ Generation of octahedral Co(III) sites in an amorphous phase was also observed to occur upon oxidative corrosion of cobalt oxide NPs with CAN (cerium ammonium nitrate), and was reported to activate the surface towards electrochemical water oxidation, see ref. 39.
§§ The apparent inertia of Co(II) sites towards oxidation to Co(III) could be associated to the expected reorganization energy due to the changes of coordination geometry (tetrahedral to octahedral) and of spin state (high spin to low spin) associated to the Co(II)→Co(III) transition.
‡ Utilization of higher formal [Co_3O_4] concentrations leads to inefficient Ru(III) photoproduction and unreliable kinetic determination due to fluctuation of the analysis beam caused by the increasing scattering. An appreciable first-order dependence on the formal Co_3O_4 concentration of the 450-nm bleach recovery was, however, previously found for Co_3O_4 NPs at concentration in the order of 10^{-4} M, see reference 13.
♦ Due to the limited time-window of our instrumental setup, at pH 8.0 and 8.5 the bleach recovery cannot be completely defined. In order to attain kinetic information, the experimental traces were fitted with linear functions, used to determine the τ.
♣ The Co(IV)=O state is often described with a partial Co(III)-O· character, see ref. 7.

1 A. Harriman, G. Porter and P. Walters, *J. Chem. Soc., Faraday Trans.*, 1981, **2**, 2373–2383.
2 S. Du, Z. Ren, J. Zhang, J. Wu, W. Xi, J. Zhu and H. Fu, *Chem. Commun.*, 2015, **51**, 8066–8069.
3 L. Wu, Q. Li, C. H. Wu, H. Zhu, A. Mendoza-Garcia, B. Shen, J. Guo and S. Sun, *J. Am. Chem. Soc.*, 2015, **137**, 7071–7074.
4 J. R. Swierk and T. D. Tilley, *J. Electrochem. Soc.*, 2018, **165**, H3028–H3033.
5 S. Jung, C. C. L. McCrory, I. M. Ferrer, J. C. Peters and T. F. Jaramillo, *J. Mater. Chem. A*, 2016, **4**, 3068–3076.
6 Z. W. She, J. Kibsgaard, C. F. Dickens, I. Chorkendorff, J. K. Nørskov and T. F. Jaramillo, *Science (80-.).*, 2017, **355**, eaad4998.
7 M. Zhang, M. De Respinis and H. Frei, *Nat. Chem.*, 2014, **6**, 362–367.
8 F. Jiao and H. Frei, *Angew. Chemie - Int. Ed.*, 2009, **48**, 1841–1844.
9 F. Jiao and H. Frei, *Energy Environ. Sci.*, 2010, **3**, 1018.
10 M. Grzelczak, J. Zhang, J. Pfrommer, J. Hartmann, M. Driess, M. Antonietti and X. Wang, *ACS Catal.*, 2013, **3**, 383–388.
11 J. Rosen, G. S. Hutchings and F. Jiao, *J. Am. Chem. Soc.*, 2013, **135**, 4516–4521.
12 N. Shi, W. Cheng, H. Zhou, T. Fan and M. Niederberger, *Chem. Commun.*, 2015, **51**, 1338–1340.
13 I. Bazzan, A. Volpe, A. Dolbecq, M. Natali, A. Sartorel, P. Mialane and M. Bonchio, *Catal. Today*, 2017, **290**, 39–50.
14 M. Natali, S. Berardi, A. Sartorel, M. Bonchio, S. Campagna and F. Scandola, *Chem. Commun.*, 2012, **48**, 8808.
15 M. Natali, M. Orlandi, S. Berardi, S. Campagna, M. Bonchio, A. Sartorel and F. Scandola, *Inorg. Chem.*, 2012, **51**, 7324–7331.
16 A. Sartorel, M. Bonchio, S. Campagna and F. Scandola, *Chem. Soc. Rev.*, 2013, **42**, 2262–2280.
17 M. Natali, I. Bazzan, S. Goberna-Ferrón, R. Al-Oweini, M. Ibrahim, B. S. Bassil, H. Dau, F. Scandola, J. R. Galán-Mascarós, U. Kortz, A. Sartorel, I. Zaharieva and M. Bonchio, *Green Chem.*, 2017, **19**, 2416–2426.
18 S. Berardi, G. La Ganga, M. Natali, I. Bazzan, F. Puntoriero, A. Sartorel, F. Scandola, S. Campagna and M. Bonchio, *J. Am. Chem. Soc.*, 2012, **134**, 11104–11107.
19 E. Pizzolato, M. Natali, B. Posocco, A. Montellano López, I. Bazzan, M. Di Valentin, P. Galloni, V. Conte, M. Bonchio, F. Scandola and A. Sartorel, *Chem. Commun.*, 2013, **49**, 9941.
20 A. Genoni, G. La Ganga, A. Volpe, F. Puntoriero, M. Di Valentin, M. Bonchio, M. Natali and A. Sartorel, *Faraday Discuss.*, , DOI:10.1039/c5fd00076a.
21 G. La Ganga, F. Puntoriero, S. Campagna, I. Bazzan, S. Berardi, M. Bonchio, A. Sartorel, M. Natali and F. Scandola, *Faraday Discuss.*, 2012, **155**, 177–190.
22 J. R. Swierk and T. E. Mallouk, *Chem. Soc. Rev.*, 2013, **42**, 2357–2387.
23 J. W. Youngblood, S. H. A. Lee, Y. Kobayashi, E. A. Hernandez-Pagan, P. G. Hoertz, T. A. Moore, A. L. Moore, D. Gust and T. E. Mallouk, *J. Am. Chem. Soc.*, 2009, **131**, 926–927.
24 A. M. Ullman, C. N. Brodsky, N. Li, S. L. Zheng and D. G. Nocera, *J. Am. Chem. Soc.*, 2016, **138**, 4229–4236.
25 J. Guan, C. Ding, R. Chen, B. Huang, X. Zhang, F. Fan, F. Zhang and C. Li, *Chem. Sci.*, 2017, **8**, 6111–6116.
26 S. J. Folkman, M. Zhou, M. Nicki and R. G. Finke, *Inorg. Chem.*, 2018, **57**, 1517–1526.
27 S. Ghosh, A. V. Soudackov and S. Hammes-Schiffer, *ACS Nano*, 2017, **11**, 10295–10302.
28 N. Song, J. J. Concepcion, R. A. Binstead, J. A. Rudd, A. K. Vannucci, C. J. Dares, M. K. Coggins and T. J. Meyer, *Proc. Natl. Acad. Sci.*, 2015, **112**, 4935–4940.
29 T. Irebo, S. Y. Reece, M. Sjdin, D. G. Nocera, L.

View Article Online
DOI: 10.1039/C8SE00275D

Hammarstrom and M. Sjo, *J. Am. Chem. Soc.*, 2007, **129**, 15462–15464.
30 D. Wang and J. T. Groves, *Proc. Natl. Acad. Sci.*, 2013, **110**, 15579–15584.
31 D. R. Weinberg, C. J. Gagliardi, J. F. Hull, C. F. Murphy, C. A. Kent, B. C. Westlake, A. Paul, D. H. Ess, D. G. McCafferty and T. J. Meyer, *Chem. Rev.*, 2012, **112**, 4016–4093.
32 J. N. Schrauben, R. Hayoun, C. N. Valdez, M. Braten, L. Fridley and J. M. Mayer, *Science (80-.).*, 2012, **336**, 1298–1301.
33 D. G. Nocera, *Acc. Chem. Res.*, 2012, **45**, 767–776.
34 W. Jencks, *Chem. Rev.*, 1972, **72**, 705–718.
35 S. Hammes-Schiffer, *J. Am. Chem. Soc.*, 2015, **137**, 8860–8871.
36 A. Yamaguchi, R. Inuzuka, T. Takashima, T. Hayashi, K. Hashimoto and R. Nakamura, *Nat. Commun.*, 2014, **5**, 1–6.
37 A. Kręzel and W. Bal, *J. Inorg. Biochem.*, 2004, **98**, 161–166.
38 T. Zhai, L. Wan, S. Sun, Q. Chen, J. Sun, Q. Xia and H. Xia, *Adv. Mater.*, 2017, **29**, 1–8.
39 A. Indra, P. W. Menezes, C. Das, C. Göbel, M. Tallarida, D. Schmeiβer and M. Driess, *J. Mater. Chem. A*, 2017, **5**, 5171–5177.

View Article Online
DOI: 10.1039/C8SE00275D

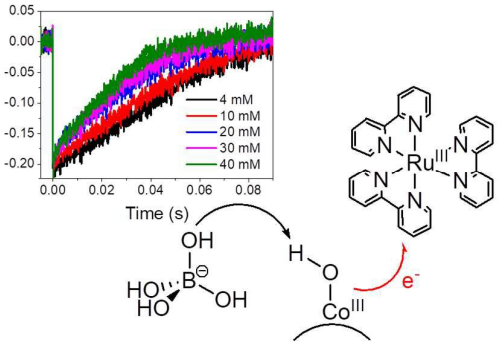

Flash photolysis studies indicate general base catalysis by borate in photoinduced proton-coupled electron transfer from Co_3O_4 nanoparticles to Ru(III)$(bpy)_3^{3+}$